nature geoscience

Article

https://doi.org/10.1038/s41561-024-01420-6

Greater climate sensitivity implied by anvil cloud thinning

Received: 24 April 2023

Accepted: 15 March 2024

Published online: 17 April 2024

Check for updates

Adam B. Sokol [1] ✉, Casey J. Wall [2] & Dennis L. Hartmann [1]

High clouds produced by tropical convection are expected to shrink in area as the climate warms, and the radiative feedback associated with this change has long been the subject of controversy. In a recent assessment of climate sensitivity, the World Climate Research Programme estimated that this feedback is substantially negative, albeit with substantial uncertainty. Here we examine the cloud response using an approach that treats high clouds as part of an optical continuum rather than entities with fixed opacity. We show that a substantial negative feedback is not supported by an ensemble of high-resolution atmospheric models. Rather, the models suggest that changes in cloud area and opacity together act as a weakly positive feedback. The positive opacity component arises from the disproportionate reduction in the area of thick, climate-cooling clouds relative to thin, climate-warming clouds. This suggests that thick cloud area is tightly coupled to the rate of convective overturning—which is expected to slow with warming—whereas thin cloud area is influenced by other, less certain processes. The positive feedback differs markedly from previous estimates and leads to a +0.3 °C shift in the median estimate of equilibrium climate sensitivity relative to a previous community assessment.

Anvil clouds produced by deep convection are widespread in the tropics and are a leading source of uncertainty in the recent assessment of climate sensitivity by the World Climate Research Programme (WCRP)[1]. Thermodynamic arguments predict that anvil cloud area decreases as the surface warms[2,3], but this could produce a positive, negative or neutral radiative feedback, because, unlike other cloud types, anvils can have either a positive or negative cloud radiative effect at different stages of their life cycle[4,5]. Deep convective towers and fresh, thick anvils have a high albedo and a strong, negative radiative effect, while thinner, aged anvils exert a modest, positive radiative effect[6]. Previous estimates of the anvil area feedback are altogether inconclusive; nevertheless, the maximum likelihood value assessed by the WCRP was substantially negative ($-0.2\ \mathrm{W\ m^{-2}\ K^{-1}}$, with a Gaussian standard deviation of $0.2\ \mathrm{W\ m^{-2}\ K^{-1}}$). Here, we will show that such a negative feedback is not supported by an ensemble of state-of-the-art cloud-resolving models (CRMs). To the contrary, the models predict that reductions in high cloud area come mostly from thick, reflective anvil clouds that cool the climate. The clouds left behind are optically thinner on average and have a more positive climatological radiative effect.

Previous work examining the relationship between surface temperature (T_s) and convective cloud area generally supports a reduction in cloud area with warming, albeit with regional and methodological sensitivities[7–17]. Estimates of the associated radiative feedback, however, range from substantially negative[11,14,18] to nearly neutral[7] or slightly positive[17,19–22]. This continued uncertainty may arise, in part, from the use of various cloud classifications (for example, cirrus, high cloud, anvil, stratiform and so on) based on arbitrary thresholds that vary from study to study. In reality, tropical convection generates a continuum of ice clouds, with thick cumulonimbi on one end and thin cirrus on the other. This continuum perspective is valuable because it reflects real physical processes—the production, gradual thinning and eventual dissipation of ice clouds—and provides an intuitive way of understanding the role of convectively generated clouds in tropical climate.

[1]Department of Atmospheric Sciences, University of Washington, Seattle, WA, USA. [2]Department of Geosciences, University of Oslo, Oslo, Norway. ✉e-mail: abs66@uw.edu

https://doi.org/10.1038/s41561-024-01420-6

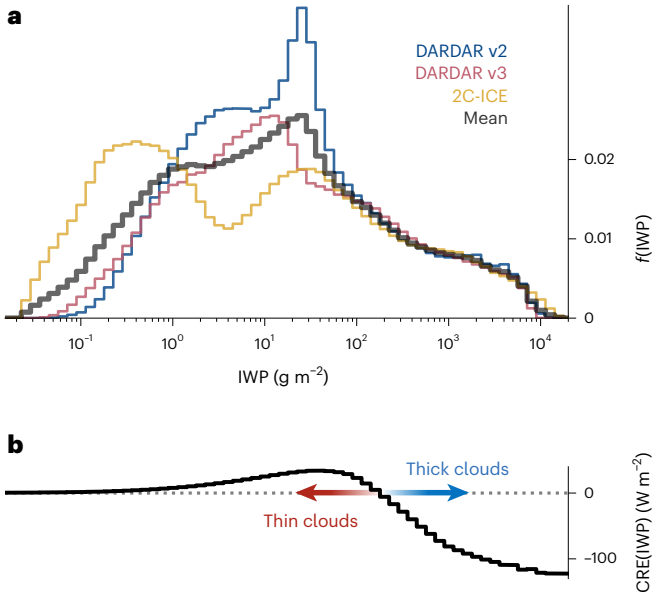

Fig. 1 | The tropical ice cloud continuum. a, f(IWP) derived from satellite observations of the tropical West Pacific (150–180° E, 15° S–15° N) for 2009. Three satellite retrievals and their mean are shown: DARDAR v2 is the DARDAR-Cloud version 2.1.1 (ref. 47); DARDAR v3 is the DARDAR-Cloud version 3.1 (ref. 48); and 2C-ICE is the 2C-ICE R05 (ref. 49) (Methods). **b**, Multimodel mean CRE(IWP) for the CRM simulations with T_s = 300 K. Low cloud effects are treated as described in the Methods.

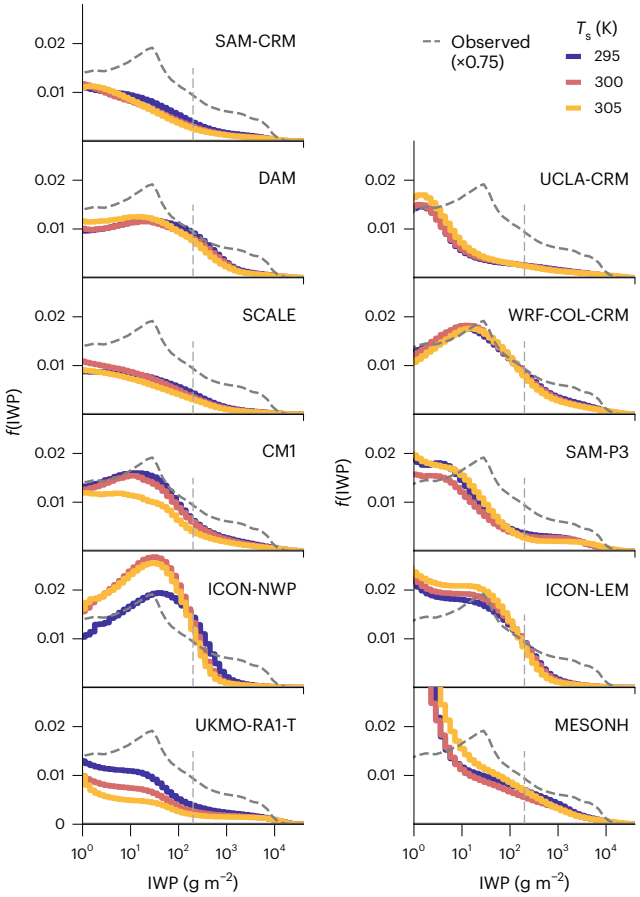

Fig. 2 | Model representations of the ice cloud continuum. f(IWP) for each model and each T_s are shown. Dashed grey lines show the mean of the three satellite-derived estimates of f, scaled arbitrarily by a factor of 0.75 to aid comparison of distribution shapes. Vertical, dashed grey lines mark the cutoff between thick and thin clouds.

Here, we examine the ice cloud continuum using ice water path (IWP) as a coordinate. IWP—the total mass of condensed ice in the atmospheric column—can be estimated from satellite observations, is easily calculated from model output, and is closely linked to cloud radiative effect and optical depth (τ; Extended Data Fig. 1). Changes in the frequency distribution of IWP are therefore informative for understanding the impact of ice clouds on the top-of-atmosphere radiative balance.

We apply the continuum perspective to an ensemble of CRMs in which deep convection and anvil evolution are explicitly simulated. As part of the Radiative–Convective Equilibrium Model Intercomparison Project (RCEMIP)[23], these models were run on a limited-area, oceanic domain large enough to permit large-scale convective organization (Methods). Simulations were conducted for three fixed, uniform T_s values (295, 300 and 305 K). We will show that the ice cloud response to warming is characterized by two regimes: a robust reduction in thick ice cloud area that is consistent with existing thermodynamic arguments and a small but uncertain change in thin ice cloud area. Such changes produce an overall thinning of the cloud population and a positive opacity feedback, implying a +0.3 °C shift in the WCRP estimate of equilibrium climate sensitivity (ECS).

Convective clouds as a continuum of ice

The continuum of tropical ice clouds can be represented by a discrete frequency distribution of IWP[24,25]. We denote this distribution as f(IWP), which can be interpreted as the IWP-resolved cloud fraction. Similarly, we denote the mean cloud radiative effect of convectively generated ice clouds as CRE(IWP) (Methods). Satellite-derived estimates of f from the tropical West Pacific, along with model-estimated CRE, provide an intuitive understanding of convective cloud evolution (Fig. 1). At high IWP (>10^3 g m^{-2}), deep convective cores have a large, negative CRE but cover a small area. As IWP decreases, f and CRE both increase rapidly, which reflects the thinning and spreading of detrained anvils. Maximum f occurs around 15–35 g m^{-2} ($\tau \approx 1$–2; Extended Data Fig. 1), which approximately coincides with the CRE maximum; the most abundant anvil clouds are therefore those with the strongest warming effect. These clouds counteract the cooling effect of thicker clouds, leading to a climatological cloud radiative effect near zero in tropical convective regions[26,27].

The CRM ensemble produces a wide variety of IWP distributions with varying degrees of similarity to the satellite-derived f (Fig. 2). In general, the models capture the maximum IWP of 2–4 × 10^4 g m^{-2} and the rapid increase in f as IWP decreases from 10^3 to 10^2 g m^{-2}. More than half of the models produce a relative maximum or plateau near the observed range of 15–35 g m^{-2}. This suggests that the models are generally capturing the basic thinning and spreading of anvil clouds after detrainment, and that the convective cloud continuum can be captured even in idealized representations of the tropical atmosphere. While the individual f(IWP) curves produced by each model vary substantially, we will show that the change in f in response to surface warming follows a robust pattern across the ensemble.

In the deep tropics, the ice cloud continuum is dominated by clouds with tops near the level of deep convective detrainment[28]. Mid-level ice clouds are very rare in the observations and model simulations considered here (Extended Data Figs. 2–3), so we are confident that f reflects a continuum of high clouds consisting of deep convective towers, their attached anvils and thin cirrus of convective or in-situ origin (Supplementary Fig. 1). Based on Fig. 1, the continuum can be divided into two categories with physical relevance for cloud–climate interactions: clouds with CRE < 0 and those with CRE > 0. We refer to these as thick and thin clouds, respectively, and separate them by

https://doi.org/10.1038/s41561-024-01420-6

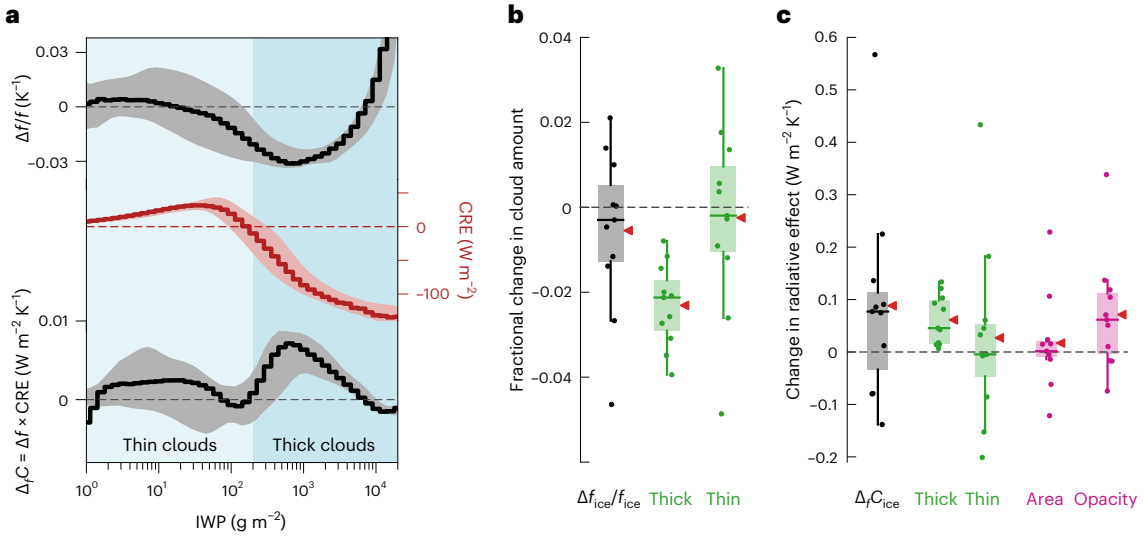

Fig. 3 | The ice cloud response to warming and its radiative effects. a, Fractional change in f(IWP), CRE(IWP) for T_s = 295 K and $\Delta_f C$, the change in domain-averaged CRE due to changes in f alone. Lines show the multimodel means and shading shows the 25–75th percentiles. **b**, Fractional change in f_{ice} and its decomposition into thick and thin cloud components. **c**, The combined area and opacity feedback $\Delta_f C_{ice}$, its thick and thin cloud components, and its area and opacity components. All changes are evaluated between 295 and 305 K and normalized by ΔT_s. For box plots, boxes show quartiles 1–3 and outliers differ from quartile 1 or 3 by at least 1.5 × interquartile range. Dashes show medians, red triangles show means and dots show individual models (n = 11).

an IWP threshold corresponding to the change in sign of the multimodel mean CRE. The area fractions covered by thick and thin clouds are then

$$f_{\text{thick}} = \sum_{200\,\text{g m}^{-2}}^{\infty} f(\text{IWP})$$

$$f_{\text{thin}} = \sum_{1\,\text{g m}^{-2}}^{200} f(\text{IWP})$$

and the total ice cloud fraction is $f_{ice} = f_{thick} + f_{thin}$. Clouds with IWP < 1 g m^{-2} have a small radiative effect and are excluded from our analysis, which does not affect our results (Supplementary Discussion 1).

The domain-averaged radiative effect of ice clouds, denoted here as C_{ice}, can be similarly decomposed into thick and thin cloud contributions, C_{thick} and C_{thin}, respectively. We first define the area-weighted CRE as

$$C(\text{IWP}) = f(\text{IWP}) \times \text{CRE}(\text{IWP}) \quad (1)$$

which represents the cloud radiative effect of a particular IWP bin averaged over the entire domain. Then, as with f, C_{ice}, C_{thick} and C_{thin} are found by summing C over the relevant IWP intervals (Methods and Extended Data Fig. 4).

Ice cloud thinning in response to warming

The response of f to surface warming varies substantially across the ensemble (Fig. 2 and Extended Data Figs. 5 and 6). To identify robust aspects of the response, we compute the multimodel mean fractional change in f between 295 and 305 K (Fig. 3a). This shows that f increases with warming at the largest IWPs, reflecting an increase in the ice content of the strongest convective updrafts. Otherwise, we find that thick clouds consistently contract across the entire ensemble, with a mean change in f_{thick} of −2% K^{-1}. This change, reflective of a decrease in the area occupied by deep convective cores and fresh anvils, is in line with the anticipated weakening of the mean convective mass flux[29–31]. In theory, this weakening could manifest as a decrease in the convective area fraction, a decrease in the vertical velocity within convection or some combination thereof. Because convective storms are expected to be more vigorous with warming[32,33], it seems likely that convective area fraction decreases. This could arise from a reduction in the number of convective events or a decrease in their typical width, but the present analysis does not discern between these two mechanisms. Regardless, the reduction in f_{thick} seen here suggests that changes in convective area fraction affect not only deep convective cores but also fresh, thick anvil clouds, which are typically attached to convective cores and undergo relatively rapid thinning after their formation[34,35]. The impressive agreement between the CRMs (Fig. 3b and Extended Data Fig. 5c) suggests that this response is rooted in fundamental physics shared by all of the models.

In contrast to the reduction in f_{thick}, there is no model consensus on changes in thin cloud area. The ensemble is evenly split on the sign of Δf_{thin}, resulting in a small ensemble mean response despite wide intermodel spread (Fig. 3b). The mismatch between changes in f_{thick} and f_{thin} suggests that the thin cloud response is not as tightly constrained by changes in the convective mass flux. This is in line with our current understanding that the spreading, thinning and maintenance of aged anvils are driven by various microphysical and radiative processes that are not directly related to the total convective mass flux[4,5,36–38]. Intermodel differences in the representation of these processes (particularly microphysics) almost certainly impact the simulated thin cloud response. With these insights into the anvil life cycle, it is perhaps unsurprising that Δf_{thin} is poorly constrained compared with Δf_{thick}. Because thin clouds are much more abundant than thick ones, changes in f_{ice} largely reflect those in f_{thin} (Supplementary Tables 1 and 2). Intermodel spread in Δf_{ice} is best explained by Δf at ~20 g m^{-2} (r^2 = 0.92; Extended Data Fig. 7), which closely corresponds to the most abundant IWP in observations and some models.

With a robust reduction in f_{thick} and a small mean change in f_{thin}, the ensemble suggests that the ice cloud population becomes thinner in response to surface warming. The ratio of thin to thick clouds increases in all but one of the models (Extended Data Fig. 6), demonstrating that this thinning can occur regardless of whether the total ice cloud fraction increases, decreases or stays the same. This thinning is qualitatively consistent with the previous finding that thick, high clouds respond more readily than thin, high clouds to interannual T_s variability observed in the real tropics[8,16,21,39,40].

https://doi.org/10.1038/s41561-024-01420-6

A positive opacity feedback

We now seek to understand how changes in the ice cloud continuum affect C_{ice}, the domain-averaged radiative effect of ice clouds. The change in C due solely to changes in f is expressed as

$$\Delta_f C(\mathrm{IWP}) = \mathrm{CRE}(\mathrm{IWP}) \times \Delta f(\mathrm{IWP}) \quad (2)$$

where Δ_f denotes the change due to f alone, normalized by ΔT_s, and CRE(IWP) is evaluated at the initial T_s. As before, $\Delta_f C_{thick}$, $\Delta_f C_{thin}$ and $\Delta_f C_{ice}$ are found by summing $\Delta_f C$ over the respective IWP intervals. $\Delta_f C_{ice}$ can be interpreted as a combined area and opacity feedback, although it neglects the part of the opacity feedback related to changes in cloud microphysics (Methods).

We assess $\Delta_f C$ and $\Delta_f C_{ice}$ separately for each model between 295 and 305 K. All but three produce positive $\Delta_f C_{ice}$ (Fig. 3c and Supplementary Table 2), demonstrating that cloud thinning can lead to an increase in climatological cloud radiative effect regardless of whether f_{ice} increases or decreases. The ensemble mean $\Delta_f C_{ice}$ is +0.09 W m^{-2} K^{-1}; nearly all of this increase comes from thick cloud changes, while the mean thin cloud contribution is again very small but with considerably more spread (Fig. 3c). Intermodel spread in $\Delta_f C_{ice}$ is well explained by its thin cloud component ($r^2 = 0.95$) and best predicted by $\Delta_f C$ at 40–70 g m^{-2} ($r^2 = 0.97$; Extended Data Figure 7).

$\Delta_f C_{ice}$ can be decomposed into two parts analogous to conventional cloud area and opacity feedbacks (Methods). The area component assumes a uniform fractional change in f and no change in $\overline{\mathrm{CRE}}$, the conditionally averaged radiative effect of ice clouds. In most of the models, the area component is very small (Fig. 3c), either because Δf_{ice} is small or because the ice cloud population is about radiatively neutral to begin with. This is in line with previous arguments suggesting that the radiative neutrality of convective clouds constrains the area feedback to be small[41].

The opacity component of $\Delta_f C_{ice}$ accounts for changes in $\overline{\mathrm{CRE}}$ brought about by non-uniform changes in f, such as the thinning of the cloud population described above. Unlike the area component, the opacity component is generally positive across the ensemble (Fig. 3c), reflecting a mean increase in $\overline{\mathrm{CRE}}$ due to cloud thinning. The ensemble mean opacity component accounts for nearly all of the magnitude of $\Delta_f C_{ice}$, suggesting that when it comes to anvil radiative feedbacks, the total change in cloud area is less important than how that change is spread across the ice cloud continuum. The CRMs show impressive agreement in this regard, as does at least one general circulation model with parameterized convection[21]. Again, intermodel spread in the area and opacity components is well explained by the spread in Δf_{thin} (Extended Data Fig. 8).

Implications for climate sensitivity

The positive feedback predicted by the CRM ensemble represents a notable departure from the WCRP estimate of the combined anvil area and opacity feedback (Supplementary Discussion 2), suggesting that clouds act to enhance global warming more than was assumed in the WCRP assessment of ECS. To update that assessment, we replace the previous feedback estimate with our RCEMIP-informed value and generate a new probability density function (PDF) of ECS. We calculate the RCEMIP-informed value by converting the multimodel mean $\Delta_f C_{ice}$ to a global mean feedback (Methods). This gives a feedback estimate of $N(0.03, 0.06)$ W m^{-2} K^{-1}, where, following the WCRP convention[1], $N(x, y)$ is a Gaussian with mean x and standard deviation y, which we set equal to the feedback standard deviation across the RCEMIP ensemble. While the RCEMIP-informed feedback is small in magnitude compared with other cloud feedbacks, it is a large change from the previous estimate and corresponds to a 51% increase in the total cloud feedback assessed by the WCRP.

Updating the feedback results in a broad +0.3 °C shift in the ECS PDF (Fig. 4). The central estimate (median) increases from 3.1 to 3.4 °C,

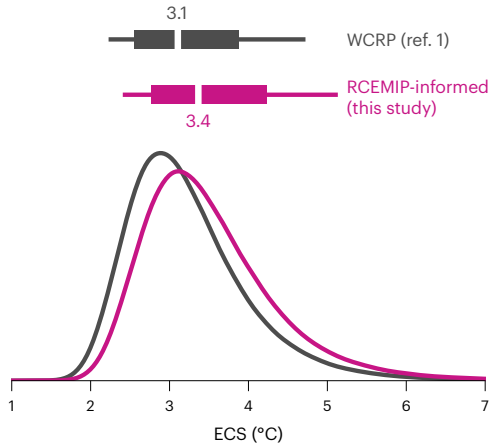

Fig. 4 | Updating the PDF of ECS. The grey line shows the WCRP baseline estimate from ref. 1, which uses an anvil area feedback of $N(-0.20, 0.20)$ W m^{-2} K^{-1}, where $N(x, y)$ is a Gaussian with mean x and standard deviation y. The pink line shows the updated calculation using the RCEMIP-informed value of $N(0.03, 0.06)$ W m^{-2} K^{-1}. The horizontal lines and boxes at the top show 90% and 66% confidence intervals, respectively, and white dashes show the central estimate (median).

and the 66% likely range from 2.6–3.9 to 2.8–4.2 °C (Extended Data Table 1). The ~10% widening of the likely range is counterintuitive given the reduction in anvil feedback uncertainty relative to the WCRP assessment. The reduction in uncertainty is outweighed by the increase in the central estimate of the feedback, which acts to broaden the PDF due to the nonlinear relationship between ECS and feedback strength[42]. The likelihoods of extreme ECS values are most dramatically affected by the feedback update: the probability of ECS > 6 °C doubles, while that of ECS < 2 °C is reduced by 74%. Sensitivity tests (Methods) show that the shift in the PDF results from the increase in the central estimate of the feedback and is quite insensitive to the feedback uncertainty (Extended Data Fig. 9 and Extended Data Table 1).

Extrapolating from RCEMIP to a global mean feedback comes with the caveat that certain atmospheric changes cannot be captured in such idealized simulation setups. For example, our feedback estimate cannot account for warming-induced changes in planetary-scale circulation or dynamical modes of variability, which could affect patterns of convection and cloudiness. However, the RCEMIP CRMs produce a wide range of changes in large-scale convective organization in response to warming[43]; these changes freely affect cloud properties and are thus implicitly included in our analysis. We are therefore confident that our estimate spans a wide range of possible changes in large-scale convective dynamics. Furthermore, we have already shown that the CRMs capture the expected reduction in deep convective area in response to warming; this, along with previous work showing that the ensemble-predicted changes in cloud altitude and temperature are consistent with observational and theoretical expectations[43,44], adds confidence that the most fundamental aspects of the convective response are well represented by the CRMs.

Thin clouds are key for reducing uncertainty

A main takeaway of this work is that changes in tropical ice cloud opacity are a critical part of the cloud response to warming. The possibility of a high cloud opacity feedback has been noted before[18,21,45] but has received comparatively little attention in broader discussions of cloud feedback and ECS. Previous assessments have often assumed fixed anvil opacity[11,20], perhaps due to the lack of a priori expectations for how changes in area would be spread across the distribution of clouds observed in the present-day tropics. By treating tropical ice clouds as a continuum, this work provides an initial characterization of that response. While our estimate of the combined area and opacity

feedback is small, it constitutes a marked increase from the WCRP estimate[1] and implies a substantial shift in the PDF of ECS.

The continuum framework has revealed that thick, climate-cooling and thin, climate-warming clouds are affected differently by changes in T_s. The robust decrease in thick cloud area mirrors expected changes in convective mass flux, whereas the uncertain thin cloud response appears to be influenced by other factors. In particular, thin clouds with IWP between 20 and 70 g m^{-2} ($\tau \approx 1$–3) are the leading source of uncertainty in changes in ice cloud area and radiative effect. These clouds are known to be shaped by various radiative, dynamic and microphysical processes that may respond to warming in complex ways[46]. Constraining these changes is a challenging undertaking that requires consideration of a wide range of physical scales, but such an endeavour may prove critical for understanding tropical climate change.

Online content

Any methods, additional references, Nature Portfolio reporting summaries, source data, extended data, supplementary information, acknowledgements, peer review information; details of author contributions and competing interests; and statements of data and code availability are available at https://doi.org/10.1038/s41561-024-01420-6.

References

1. Sherwood, S. C. et al. An assessment of Earth's climate sensitivity using multiple lines of evidence. *Rev. Geophys.* https://doi.org/10.1029/2019RG000678 (2020).
2. Zelinka, M. D. & Hartmann, D. L. Why is longwave cloud feedback positive? *J. Geophys. Res.* https://doi.org/10.1029/2010JD013817 (2010).
3. Bony, S. et al. Thermodynamic control of anvil cloud amount. *Proc. Natl Acad. Sci. USA* **113**, 8927–8932 (2016).
4. Hartmann, D. L., Gasparini, B., Berry, S. E. & Blossey, P. N. The life cycle and net radiative effect of tropical anvil clouds. *J. Adv. Model. Earth Syst.* **10**, 3012–3029 (2018).
5. Gasparini, B., Blossey, P. N., Hartmann, D. L., Lin, G. & Fan, J. What drives the life cycle of tropical anvil clouds? *J. Adv. Model. Earth Syst.* **11**, 2586–2605 (2019).
6. Hartmann, D. L. & Berry, S. E. The balanced radiative effect of tropical anvil clouds. *J. Geophys. Res.* **122**, 5003–5020 (2017).
7. Ito, M. & Masunaga, H. Process-level assessment of the iris effect over tropical oceans. *Geophys. Res. Lett.* **49**, e2022GL097997 (2022).
8. Kubar, T. L. & Jiang, J. H. Net cloud thinning, low-level cloud diminishment, and Hadley circulation weakening of precipitating clouds with tropical West Pacific SST using MISR and other satellite and reanalysis data. *Remote Sens.* **11**, 1250 (2019).
9. Saint-Lu, M., Bony, S. & Dufresne, J.-L. Observational evidence for a stability iris effect in the tropics. *Geophys. Res. Lett.* https://doi.org/10.1029/2020GL089059 (2020).
10. Saint-Lu, M., Bony, S. & Dufresne, J.-L. Clear-sky control of anvils in response to increased CO_2 or surface warming or volcanic eruptions. *NPJ Clim. Atmos. Sci.* **5**, 78 (2022).
11. Lindzen, R. S., Chou, M. D. & Hou, A. Y. Does the Earth have an adaptive infrared iris? *Bull. Am. Meteorol. Soc.* **82**, 417–432 (2001).
12. Su, H. et al. Variations of tropical upper tropospheric clouds with sea surface temperature and implications for radiative effects. *J. Geophys. Res.* https://doi.org/10.1029/2007JD009624 (2008).
13. Zelinka, M. D. & Hartmann, D. L. The observed sensitivity of high clouds to mean surface temperature anomalies in the tropics. *J. Geophys. Res.* https://doi.org/10.1029/2011JD016459 (2011).
14. Choi, Y.-S. et al. Revisiting the iris effect of tropical cirrus clouds with TRMM and A-Train satellite data. *J. Geophys. Res.* **122**, 5917–5931 (2017).
15. Igel, M. R., Drager, A. J. & van den Heever, S. C. A CloudSat cloud object partitioning technique and assessment and integration of deep convective anvil sensitivities to sea surface temperature. *J. Geophys. Res.* **119**, 10515–10535 (2014).
16. Liu, R. et al. High cloud variations with surface temperature from 2002 to 2015: contributions to atmospheric radiative cooling rate and precipitation changes. *J. Geophys. Res.* **122**, 5457–5471 (2017).
17. McKim, B., Bony, S. & Dufresne, J.-L. Physical and observational constraints on the anvil cloud feedback. Preprint at *Authorea* https://doi.org/10.22541/au.167769953.39966398/v2 (2023).
18. Mauritsen, T. & Stevens, B. Missing iris effect as a possible cause of muted hydrological change and high climate sensitivity in models. *Nat. Geosci.* **8**, 346–351 (2015).
19. Chambers, L. H., Lin, B. & Young, D. F. Examination of new CERES data for evidence of tropical iris feedback. *J. Clim.* **15**, 3719–3726 (2002).
20. Lin, B., Wielicki, B. A., Chambers, L. H., Hu, Y. & Xu, K.-M. The iris hypothesis: a negative or positive cloud feedback? *J. Clim.* **15**, 3–7 (2002).
21. Li, R. L., Storelvmo, T., Fedorov, A. V. & Choi, Y.-S. A positive iris feedback: insights from climate simulations with temperature-sensitive cloud-rain conversion. *J. Clim.* **32**, 5305–5324 (2019).
22. Williams, I. N. & Pierrehumbert, R. T. Observational evidence against strongly stabilizing tropical cloud feedbacks. *Geophys. Res. Lett.* **44**, 1503–1510 (2017).
23. Wing, A. A. et al. Radiative–convective equilibrium model intercomparison project. *Geosci. Model Dev.* **11**, 793–813 (2018).
24. Berry, E. & Mace, G. G. Cloud properties and radiative effects of the Asian summer monsoon derived from A-Train data. *J. Geophys. Res.* **119**, 9492–9508 (2014).
25. Chen, Y.-W. et al. High cloud responses to global warming simulated by two different cloud microphysics schemes implemented in the Nonhydrostatic Icosahedral Atmospheric Model (NICAM). *J. Clim.* **29**, 5949–5964 (2016).
26. Ramanathan, V. et al. Cloud-radiative forcing and climate: results from the Earth radiation budget experiment. *Science* **243**, 57–63 (1989).
27. Hartmann, D. L., Moy, L. A. & Fu, Q. Tropical convection and the energy balance at the top of the atmosphere. *J. Clim.* **14**, 4495–4511 (2001).
28. Stephens, G. et al. CloudSat and CALIPSO within the A-Train: ten years of actively observing the Earth system. *Bull. Am. Meteorol. Soc.* **99**, 569–581 (2018).
29. Knutson, T. R. & Manabe, S. Time-mean response over the tropical Pacific to increased CO_2 in a coupled ocean–atmosphere model. *J. Clim.* **8**, 2181–2199 (1995).
30. Held, I. M. & Soden, B. J. Robust responses of the hydrological cycle to global warming. *J. Clim.* **19**, 5686–5699 (2006).
31. Jeevanjee, N. Three rules for the decrease of tropical convection with global warming. *J. Adv. Model. Earth Syst.* **14**, e2022MS003285 (2022).
32. Singh, M. S., Kuang, Z., Maloney, E. D., Hannah, W. M. & Wolding, B. O. Increasing potential for intense tropical and subtropical thunderstorms under global warming. *Proc. Natl Acad. Sci. USA* **114**, 11657–11662 (2017).
33. Romps, D. M. Clausius–Clapeyron scaling of CAPE from analytical solutions to RCE. *J. Atmos. Sci.* **73**, 3719–3737 (2016).
34. Lilly, D. K. Cirrus outflow dynamics. *J. Atmos. Sci.* **45**, 1594–1605 (1988).
35. Jensen, E. J., van den Heever, S. C. & Grant, L. D. The life cycles of ice crystals detrained from the tops of deep convection. *J. Geophys. Res.* **123**, 9624–9634 (2018).

36. Schmidt, C. T. & Garrett, T. J. A simple framework for the dynamic response of cirrus clouds to local diabatic radiative heating. *J. Atmos. Sci.* **70**, 1409–1422 (2013).
37. Wall, C. J. et al. Observational evidence that radiative heating modifies the life cycle of tropical anvil clouds. *J. Clim.* **33**, 8621–8640 (2020).
38. Dobbie, S. & Jonas, P. Radiative influences on the structure and lifetime of cirrus clouds. *Q. J. R. Meteorol. Soc.* **127**, 2663–2682 (2001).
39. Höjgård-Olsen, E., Chepfer, H. & Brogniez, H. Satellite observed sensitivity of tropical clouds and moisture to sea surface temperature on various time and space scales: 1. Focus on high level cloud situations over ocean. *J. Geophys. Res.* **127**, e2021JD035438 (2022).
40. Stubenrauch, C. J., Caria, G., Protopapadaki, S. E. & Hemmer, F. 3D radiative heating of tropical upper tropospheric cloud systems derived from synergistic A-Train observations and machine learning. *Atmos. Chem. Phys.* **21**, 1015–1034 (2021).
41. Pierrehumbert, R. T. Thermostats, radiator fins, and the local runaway greenhouse. *J. Atmos. Sci.* **52**, 1784–1806 (1995).
42. Roe, G. H. & Baker, M. B. Why is climate sensitivity so unpredictable? *Science* **318**, 629–632 (2007).
43. Wing, A. A. et al. Clouds and convective self-aggregation in a multi-model ensemble of radiative-convective equilibrium simulations. *J. Adv. Model. Earth Syst.* https://doi.org/10.1029/2020MS002138 (2020).
44. Stauffer, C. L. & Wing, A. A. Properties, changes, and controls of deep-convecting clouds in radiative-convective equilibrium. *J. Adv. Model. Earth Syst.* **14**, e2021MS002917 (2022).
45. Hartmann, D. L. Tropical anvil clouds and climate sensitivity. *Proc. Natl Acad. Sci. USA* **113**, 8897–8899 (2016).
46. Gasparini, B. et al. Opinion: tropical cirrus—from micro-scale processes to climate-scale impacts. *Atmos. Chem. Phys.* **23**, 15413–15444 (2023).
47. Delanoë, J. & Hogan, R. J. Combined CloudSat–CALIPSO–MODIS retrievals of the properties of ice clouds. *J. Geophys. Res.* https://doi.org/10.1029/2009JD012346 (2010).
48. Cazenave, Q. et al. Evolution of DARDAR-CLOUD ice cloud retrievals: new parameters and impacts on the retrieved microphysical properties. *Atmos. Meas. Tech.* **12**, 2819–2835 (2019).
49. Deng, M., Mace, G. G., Wang, Z. & Okamoto, H. Tropical Composition, Cloud and Climate Coupling Experiment validation for cirrus cloud profiling retrieval using CloudSat radar and CALIPSO lidar. *J. Geophys. Res.* https://doi.org/10.1029/2009JD013104 (2010).

Methods

Satellite observations of IWP

The three satellite retrievals shown in Fig. 1a are combined radar–lidar retrievals that use measurements from the CALIOP lidar[50] and the CloudSat radar[51]. Both instruments are part of the A-Train satellite constellation. The three retrievals are DARDAR-Cloud version 2.1.1 (ref. 47), DARDAR-Cloud version 3.1 (ref. 48) and 2C-ICE R05 (ref. 49). The two versions of DARDAR-Cloud differ principally in their treatment of cloudy volumes detected by the lidar only[48].

CRM ensemble

We use output from the 'RCE_large' simulations of RCEMIP. The full simulation protocol is described in ref. 23. Briefly, the simulations have a domain size of ~6,000 × 400 km^2 with 3 km horizontal resolution. They used three fixed, uniform sea surface temperatures (295, 300 and 305 K) and were integrated for 100 days. We use the instantaneous three-dimensional output (every 6 hours) from the last 25 days of each run. Instantaneous IWP is computed by vertically integrating the total (precipitating and non-precipitating) atmospheric ice content. We included precipitating ice to be consistent with the satellite observations, which do not distinguish between ice types.

Our analysis includes all of the RCEMIP CRMs for which the necessary, standardized output is publicly available, with the exception of UKMO-RA1-T-nocloud and UKMO-CASIM. UKMO-RA1-T-nocloud is the same as UKMO-RA1-T apart from its deactivation of a subgrid cloud scheme. UKMO-CASIM is excluded because the unique vertical structure of convection in that model produces an IWP distribution that does not reflect deep convective cloud climatology, but rather expansive, stratiform ice clouds produced by convective detrainment near the freezing level. We also include the RCEMIP_large-style simulations described in ref. 52, which use the SAM model[53] with P3 microphysics[54] (referred to as SAM-P3).

Calculation of CRE(IWP) and treatment of low clouds

For each column of model output, cloud radiative effect is computed as the difference between hourly mean all-sky and clear-sky radiative fluxes. We seek to calculate CRE(IWP) such that it reflects the radiative effects of clouds produced by deep convection while excluding the effects of unrelated liquid clouds below. To this end, we first compute the mean cloud radiative effect of all columns falling within each IWP bin (the 'all-sky' cloud radiative effect) as well as that of the columns with liquid water path below 1 g m^{-2} (the 'ice-only' cloud radiative effect). Liquid clouds found in low-IWP columns are typically low clouds at the top of the boundary layer, which are unrelated to the overlying ice clouds but nevertheless have an impact on the top-of-atmosphere CRE[55]. Therefore, to exclude their radiative effects from CRE(IWP), we set CRE(IWP) equal to the ice-only cloud radiative effect for IWP < 10^2 g m^{-2}. On the other hand, liquid found in high-IWP columns is typically part of same deep convective cloud as the ice above; we seek to include these liquid effects and therefore set CRE(IWP) equal to the all-sky cloud radiative effect for IWP > 10^3 g m^{-2}. Between 10^2 and 10^3 g m^{-2}, we use a transition that is linear with respect to $\log_{10}$IWP (Supplementary Fig. 2). These thresholds were selected based on the multimodel mean liquid cloud fraction within each IWP bin (Supplementary Fig. 3), which increases rapidly within this range, signalling a shift from low clouds unrelated to the high clouds above to deep convective clouds occupying a large portion of the atmospheric column. Our results are not sensitive to the details of this transition, and the multimodel mean CRE(IWP) for T_s = 295 K changes sign at ~200 g m^{-2} ($\tau \approx 4$–5; Extended Data Fig. 1), which is consistent with previous analyses[24,56,57].

Definitions in the IWP framework

We have defined f(IWP) and CRE(IWP) as the IWP-resolved cloud fraction and radiative effect, respectively. We have also defined the area-weighted cloud radiative effect as C(IWP) = f(IWP) × CRE(IWP). For any parameter X(IWP), we compute the thick and thin cloud contributions to the domain mean as

$$X_{\text{thick}} = \sum_{200\,\text{g m}^{-2}}^{\infty} X$$

$$X_{\text{thin}} = \sum_{1\,\text{g m}^{-2}}^{200} X$$

and the total ice cloud contribution as $X_{\text{ice}} = X_{\text{thick}} + X_{\text{thin}}$. This notation is applied to f(IWP) and C(IWP) throughout the paper, with f_{ice} and C_{ice} thus representing the domain-averaged ice cloud fraction and the domain-averaged ice cloud radiative effect, respectively. The conditionally averaged ice cloud radiative effect is defined as $\overline{\text{CRE}} = C_{\text{ice}}/f_{\text{ice}}$.

Analytical expressions for cloud feedback in the IWP framework

The Cess-type cloud feedback is defined as the change in domain-averaged cloud radiative effect normalized by ΔT_s (ref. 58). It differs slightly from the formal cloud feedback parameter computed by partial radiative perturbation[59]. In traditional feedback analysis, the total cloud feedback is often decomposed into cloud altitude, area and opacity components. Resolved across the IWP continuum, the total Cess-type ice cloud feedback is expressed as

$$\Delta C(\text{IWP}) = \text{CRE} \times \Delta f + f \times \Delta\text{CRE} + \Delta f \times \Delta\text{CRE} \quad (3)$$

where all variables are functions of IWP and all Δ terms are assumed to be normalized by ΔT_s. The final term on the right-hand side is a small nonlinear term that we neglect here. The second term on the right-hand side accounts for changes in CRE(IWP), which may occur due to changes in clear-sky fluxes or cloud temperature, altitude and microphysical structure. This term encompasses so-called cloud masking effects[59], the entire ice cloud altitude feedback, as well as the microphysical part of the opacity feedback, which manifests as a change in the optical depth associated with a particular IWP. While this term is of substantial magnitude (Supplementary Fig. 4), it is not our focus here.

The first term on the right-hand side of equation (3), which we define as $\Delta_f C$, is the part of ΔC attributable to changes in the frequency of a particular IWP. $\Delta_f C_{\text{ice}}$, equal to the sum of $\Delta_f C$ across all IWP > 1 g m^{-2}, is thus the change in the domain-averaged radiative effect of ice clouds due to changes in f alone. $\Delta_f C_{\text{ice}}$ encompasses the entire ice cloud area feedback and the remaining part of the ice cloud opacity feedback, because non-uniform changes in f can drive changes in mean ice cloud opacity. To formally separate the area and opacity components, we first define the fractional change in f(IWP) as g(IWP):

$$g(\text{IWP}) = \frac{\Delta f}{f} \quad (4)$$

which can be decomposed as

$$g(\text{IWP}) = G + g'(\text{IWP}) \quad (5)$$

where $G = \Delta f_{\text{ice}}/f_{\text{ice}}$ is the fractional change in total ice cloud fraction and g' is the deviation from G at a particular IWP. Combining equations (4) and (5) yields

$$\Delta f = f \times (G + g') \quad (6)$$

which when substituted into equation (2) yields

$$\Delta_f C = C(G + g') \quad (7)$$

where we have employed equation (1). $\Delta_f C_{ice}$ is then found by summing over all IWP > 1 g m^{-2}:

$$\Delta_f C_{ice} = G \sum_{1\,g\,m^{-2}}^{\infty} C + \sum_{1\,g\,m^{-2}}^{\infty} g' C \quad (8)$$

which, using the definitions of C_{ice} and G, simplifies to

$$\Delta_f C_{ice} = \Delta f_{ice} \times \overline{CRE} + \sum_{1\,g\,m^{-2}}^{\infty} g' C \quad (9)$$

The first term on the right-hand side is the area component of $\Delta_f C_{ice}$, which is attributable to changes in total ice cloud fraction assuming fixed $\overline{CRE}$ (that is, a uniform fractional change in f across all IWP). The second term is the opacity component, which accounts for deviations from a uniform fractional change, which causes bulk thinning or thickening of the ice cloud population and may affect $\overline{CRE}$. The opacity component does not account for the microphysically driven opacity changes included in the second term of equation (3).

Recently, a simplified expression for the anvil cloud area feedback was developed[17] (equation 9, in ref. 17, which the authors refer to as the iris feedback). Unlike the Cess-type feedbacks discussed above, their expression aligns with traditional feedback formalism. Discretizing their expression shows that it is the same as the cloud area component of equation (9), with the addition of a cloud overlap term. Therefore, $\Delta_f C_{ice}$ can be interpreted as the sum of the ice cloud area feedback and the part of the opacity feedback related to changes in f. With regard to our treatment of cloud overlap here, the formulation of CRE(IWP) described above must be kept in mind. Whether or not the radiative effects of cloud liquid are included in $\Delta_f C$ depends on IWP. At high IWPs corresponding to deep convective cores and very thick anvil clouds, we have assumed that any liquid present in the column belongs to the same cloud system as the ice, and the all-sky radiative effect is thus used to evaluate $\Delta_f C$. On the other hand, at low IWPs, $\Delta_f C$ is evaluated using the ice-only radiative effect. This means, for example, that the ice-free area exposed by a reduction in f is partially occupied by low clouds exerting a negative radiative effect. The low-cloud radiative effect in the newly exposed regions is assumed to be equal to the difference between the all-sky and ice-only radiative effects. This is probably an underestimate, because the radiative effects of overlapping low and high clouds are not simply additive in reality. However, the impact of this bias on $\Delta_f C_{ice}$ is small due to compensating effects of models with increasing and decreasing thin cloud area. To account for this potential uncertainty, our analysis of ECS includes sensitivity tests, described below.

Converting $\Delta_f C_{ice}$ to a global mean feedback and estimating ECS

The ensemble mean $\Delta_f C_{ice}$ represents the anvil cloud area and opacity feedback, which we take to be valid over Earth's tropical oceans. To convert this to a global mean feedback, we multiply by the fractional area of the tropical oceans (37%) and assume that the tropics warm by 0.9 °C for every degree of global mean warming[60]. This results in the reported feedback value of $N(0.03, 0.06)$ W m^{-2} K^{-1}, where the Gaussian standard deviation is set equal to the standard deviation of the feedback across the RCEMIP ensemble. We then generated an updated PDF of ECS using the Bayesian inference code from ref. 1 with all three lines of evidence used in their original analysis (historical, process-based and palaeoclimatological).

We conduct sensitivity tests to account for additional sources of uncertainty that may not be captured by the standard deviation of the RCEMIP ensemble. For example, changes in cloud microphysical structure could contribute to the opacity feedback but are not included in our estimate due to model output limitations. Overlap between high and low clouds, some of which is accounted for in our estimate, is another possible source of model bias and feedback uncertainty. To assess the impact of greater feedback uncertainty, we run the ECS calculations for additional feedback values of $N(0.03, 0.16)$ and $N(0.03, 0.20)$ W m^{-2} K^{-1}. The value of 0.16 W m^{-2} K^{-1} is the maximum deviation of any individual model from the multimodel mean and thus encompasses the full ensemble spread. The value of 0.20 W m^{-2} K^{-1} is the WCRP-assessed uncertainty from ref. 1, intended to serve as an upper bound. As shown in Extended Data Fig. 9 and Supplementary Table 3, the resulting PDFs are very similar to the PDF for $N(0.03, 0.06)$.

Data availability

The DARDAR-Cloud satellite products are available at https://www.icare.univ-lille.fr/dardar/data-access/ and the 2C-ICE products at https://www.cloudsat.cira.colostate.edu/data-products/2c-ice. RCEMIP model output is publicly available at http://hdl.handle.net/21.14101/d4beee8e-6996-453e-bbd1-ff53b6874c0e, and output from the SAM-P3 model runs is available from the corresponding author on request. The derived statistics needed to reproduce the figures in this paper, as well as output from the SAM-P3 model runs, is available at https://doi.org/10.5281/zenodo.10640752 (ref. 61).

Code availability

The code used for the climate sensitivity calculations is available from the WCRP at https://zenodo.org/record/3945276#.ZFvtAOzMJ8Z (ref. 62). The code needed to generate the figures in this paper is available at https://doi.org/10.5281/zenodo.10640752 (ref. 61).

References

50. Winker, D. M. et al. Overview of the CALIPSO mission and CALIOP data processing algorithms. *J. Atmos. Ocean. Technol.* **26**, 2310–2323 (2009).
51. Stephens, G. L. et al. The CloudSat mission and the A-Train: a new dimension of space-based observations of clouds and precipitation. *Bull. Am. Meteorol. Soc.* **83**, 1771–1790 (2002).
52. Sokol, A. B. & Hartmann, D. L. Congestus mode invigoration by convective aggregation in simulations of radiative-convective equilibrium. *J. Adv. Model. Earth Syst.* https://doi.org/10.1029/2022MS003045 (2022).
53. Khairoutdinov, M. F. & Randall, D. A. Cloud resolving modeling of the ARM summer 1997 IOP: model formulation, results, uncertainties, and sensitivities. *J. Atmos. Sci.* **60**, 607–625 (2003).
54. Morrison, H. et al. Parameterization of cloud microphysics based on the prediction of bulk ice particle properties. Part II: case study comparisons with observations and other schemes. *J. Atmos. Sci.* **72**, 312–339 (2015).
55. Kang, H., Choi, Y.-S., Hwang, J. & Kim, H.-S. On the cloud radiative effect for tropical high clouds overlying low clouds. *Geosci. Lett.* **7**, 7 (2020).
56. Hong, Y., Liu, G. & Li, J.-L. F. Assessing the radiative effects of global ice clouds based on CloudSat and CALIPSO measurements. *J. Clim.* **29**, 7651–7674 (2016).
57. Kubar, T. L., Hartmann, D. L. & Wood, R. Radiative and convective driving of tropical high clouds. *J. Clim.* **20**, 5510–5526 (2007).
58. Cess, R. D. & Potter, G. L. A methodology for understanding and intercomparing atmospheric climate feedback processes in general circulation models. *J. Geophys. Res.* **93**, 8305–8314 (1988).
59. Soden, B. J., Broccoli, A. J. & Hemler, R. S. On the use of cloud forcing to estimate cloud feedback. *J. Clim.* **17**, 3661–3665 (2004).
60. Lee, J.-Y. et al. in *Climate Change 2021: The Physical Science Basis* (eds Masson-Delmotte, V. et al.) 553–672 (IPCC, Cambridge Univ. Press, 2021).

61. Sokol, A. B. Code & data to accompany "Greater climate sensitivity implied by anvil cloud thinning" by Sokol et al. (2024). *Zenodo* https://doi.org/10.5281/zenodo.10640752 (2024).
62. Webb, M. Code and data for WCRP climate sensitivity assessment (corrected version, December 2022). *Zenodo* https://doi.org/10.5281/zenodo.3945275 (2022).

Acknowledgements

We thank C. Stauffer for processing and sharing RCEMIP data, L. Hahn for helpful feedback on this manuscript and J. Deutloff for helpful conversations about the treatment of cloud overlap. We acknowledge the many scientists who provided simulations for RCEMIP and the German Climate Computing Center (DKRZ) for hosting the standardized RCEMIP data. This work was supported by NASA FINESST grant 80NSSC20K1613 (A.B.S. and D.L.H.) and NSF grant AGS-2124496 (D.L.H.).

Author contributions

A.B.S. conceived the project, conducted the analysis, generated the figures and wrote the manuscript. C.J.W. ran the equilibrium climate sensitivity code and provided interpretation. D.L.H. interpreted results, contributed to manuscript revision and supervised all aspects of the project.

Competing interests

The authors declare no competing interests.

Additional information

Extended data is available for this paper at https://doi.org/10.1038/s41561-024-01420-6.

Supplementary information The online version contains supplementary material available at https://doi.org/10.1038/s41561-024-01420-6.

Correspondence and requests for materials should be addressed to Adam B. Sokol.

Peer review information *Nature Geoscience* thanks Brian Soden, Claudia Stubenrauch and Aiko Voigt for their contribution to the peer review of this work. Primary Handling Editor: Tom Richardson, in collaboration with the *Nature Geoscience* team.

https://doi.org/10.1038/s41561-024-01420-6

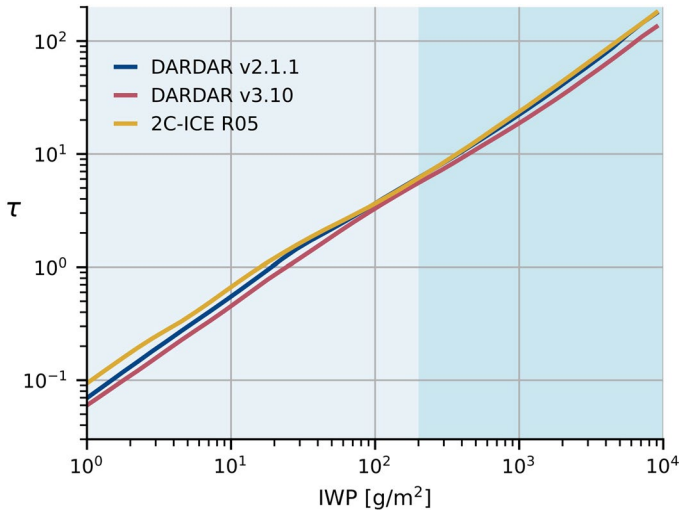

Extended Data Fig. 1 | Relationship between IWP and optical depth. Mean ice cloud optical depth τ as a function of IWP in the three combined radar-lidar satellite retrievals.

https://doi.org/10.1038/s41561-024-01420-6

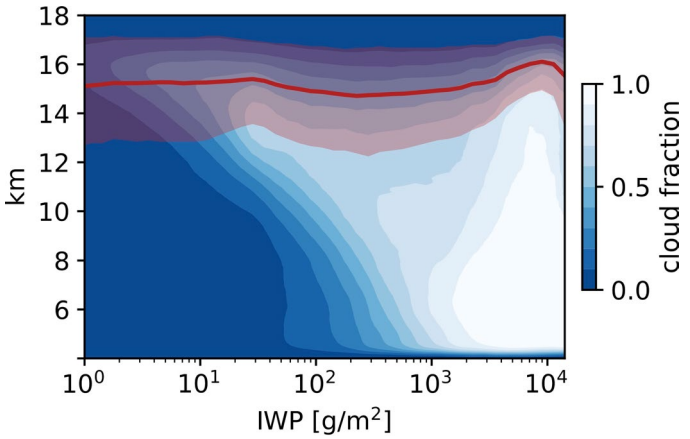

Extended Data Fig. 2 | Observed cloud macrophysical properties in IWP space. Cloud fraction composited by IWP and height in DARDAR v2.1.1. The red line shows the mean cloud top height at each IWP, with red shading between the 10th and 90th cloud top height percentiles. Following ref. 50, cloudy volumes are defined as those with nonzero ice water content and visible extinction coefficient exceeding 0.125 km^{-1}. Data are for 150-180°E and 12°S-12°N for the 2009 calendar year.

https://doi.org/10.1038/s41561-024-01420-6

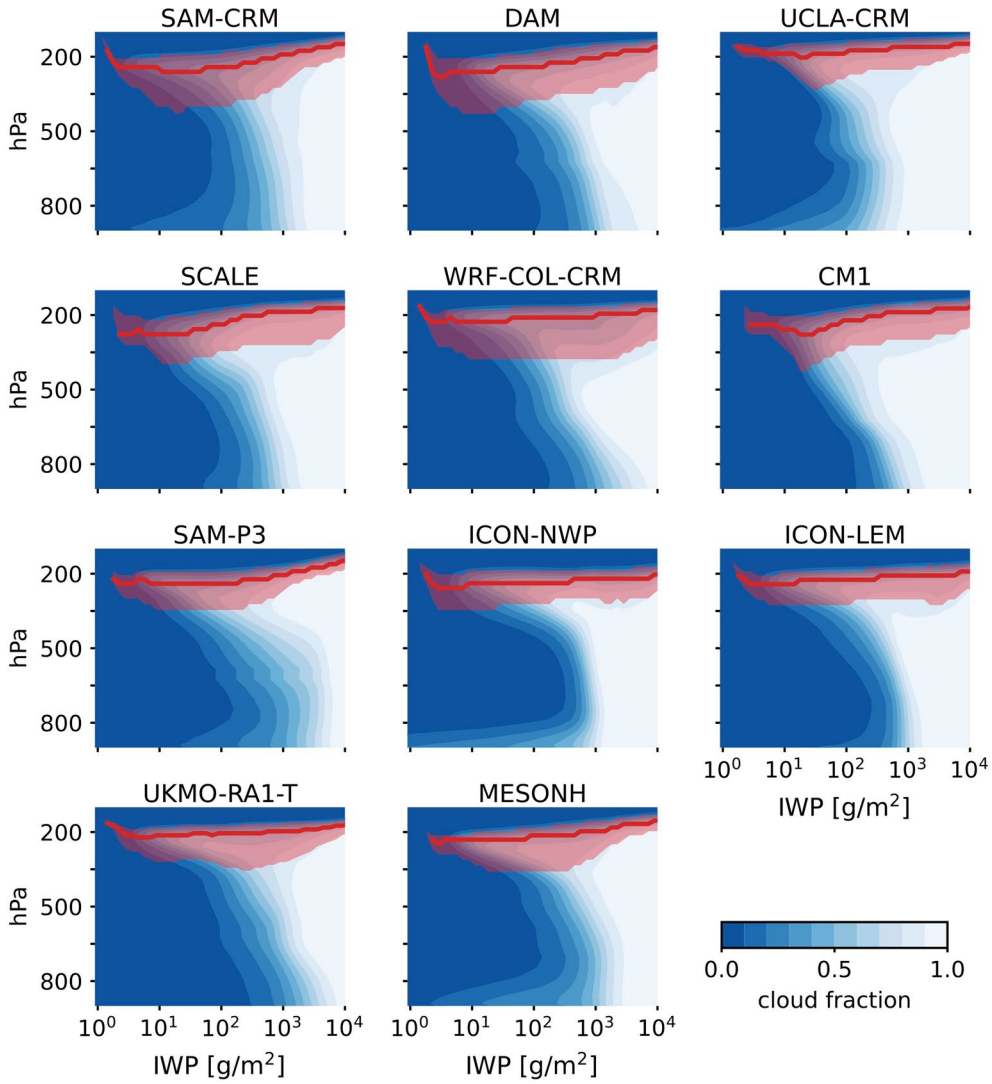

Extended Data Fig. 3 | Modeled cloud macrophysical properties in IWP space. Cloud fraction composited by pressure and IWP for the final 15 days of the RCEMIP simulations with T_s = 300 K. Grid boxes are considered cloudy if the total condensate mixing ratio exceeds 10^{-5} kg/kg. Red lines show the median cloud top pressure (CTP) of ice clouds, with red shading between the 10th and 90th CTP percentiles. The CTP statistics do not extend all the way down to IWP=1 g/m^2 because such low IWPs can only result from ice mixing ratios below the cloudiness threshold.

https://doi.org/10.1038/s41561-024-01420-6

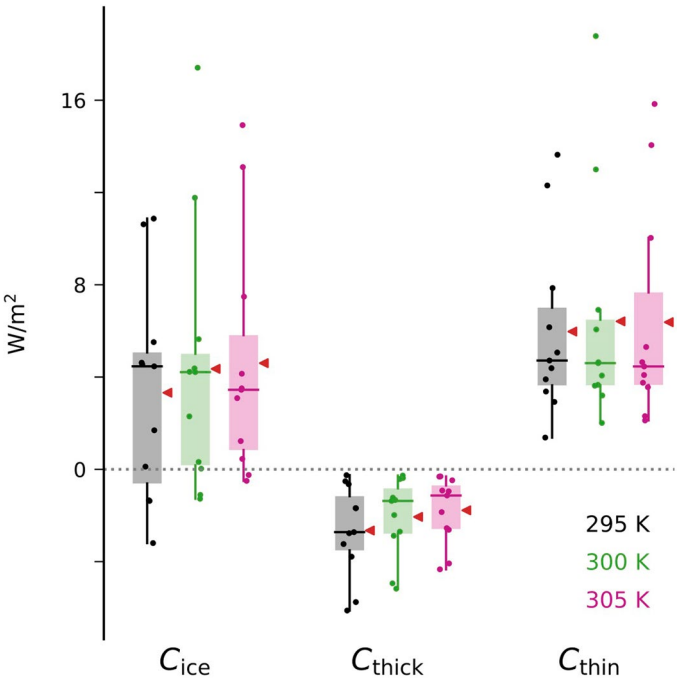

Extended Data Fig. 4 | Mean cloud radiative effects across the RCEMIP ensemble. Box plots of C_{ice}, C_{thick}, and C_{thin} in the CRM ensemble for each value of T_s. Boxes show Q1-Q3, the horizontal lines within each box show medians, red triangles show means, and each dot shows an individual model (n = 11). Outliers are defined as points that differ from Q1 or Q3 by more than 1.5x the interquartile range.

https://doi.org/10.1038/s41561-024-01420-6

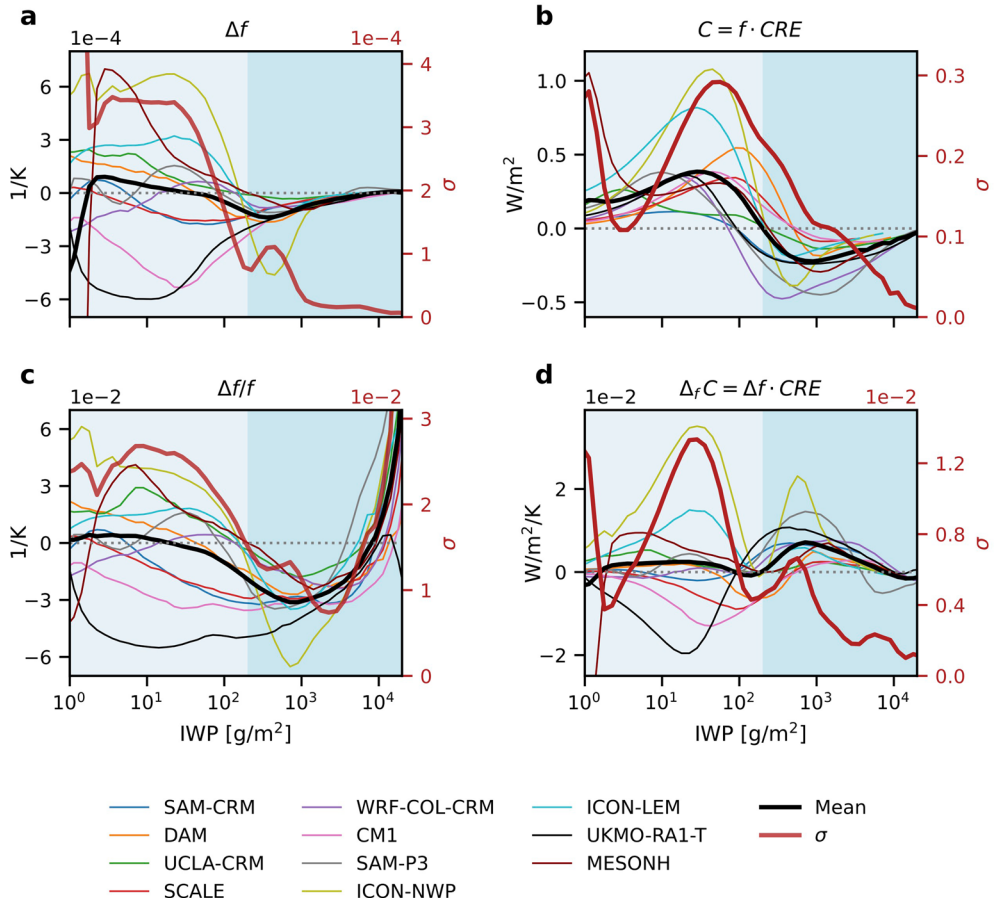

Extended Data Fig. 5 | Results for individual RCEMIP models. (a) Absolute and (c) fractional changes in f between 295 and 305 K, normalized by ΔT_s. (b) C at 295 K and (d) $\Delta_f C$ between 295 and 305 K. Thin lines show individual models. Heavy black lines show multimodel means. Heavy red lines show the ensemble standard deviation and are plotted on a different vertical axis shown in red on the right side of each plot.

https://doi.org/10.1038/s41561-024-01420-6

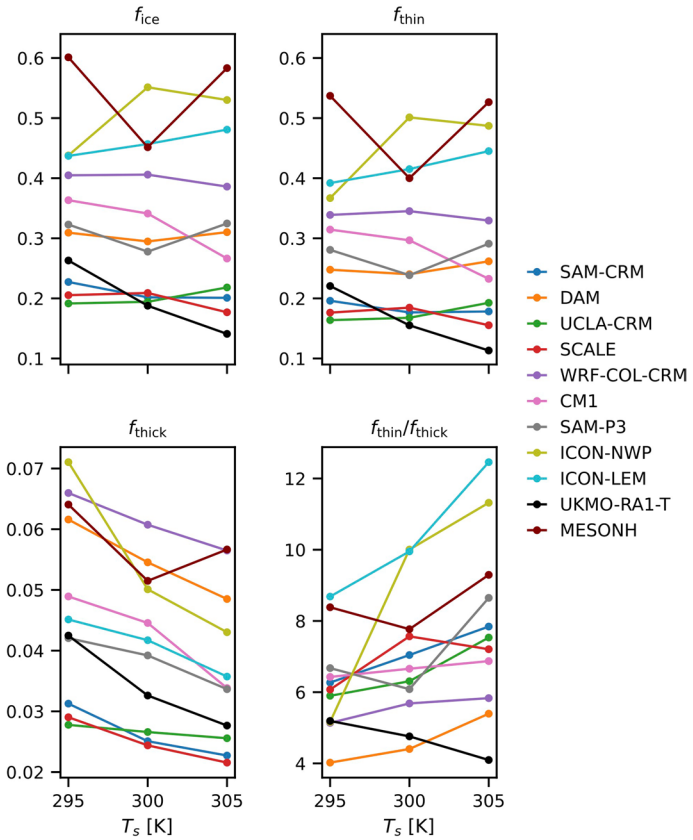

Extended Data Fig. 6 | Cloud fraction statistics for individual models. Cloud fraction as a function of T_s for each model in the CRM ensemble. Panels are shown for different portions of the IWP continuum. The bottom-right shows the ratio of thin to thick ice clouds.

https://doi.org/10.1038/s41561-024-01420-6

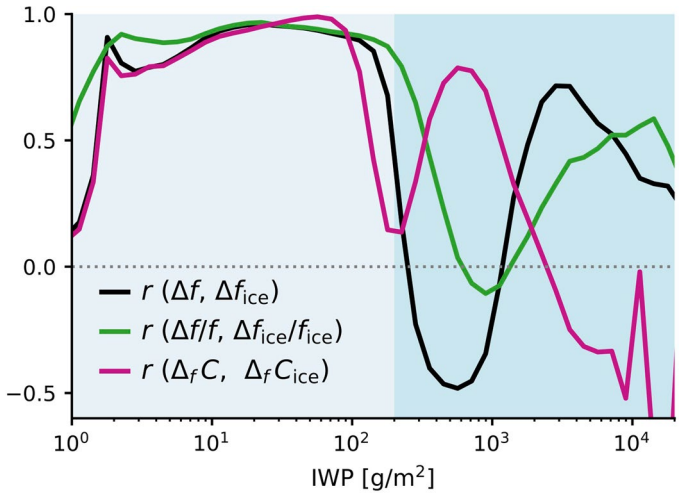

Extended Data Fig. 7 | Correlation coefficients between IWP-resolved and domain-averaged quantities. Correlation coefficients are shown for various quantities. Black: absolute changes in f(IWP) and f_{ice}. Green: fractional changes in f(IWP) and f_{ice}. Pink: $\Delta_f C$ (IWP) and $\Delta_f C_{ice}$.

https://doi.org/10.1038/s41561-024-01420-6

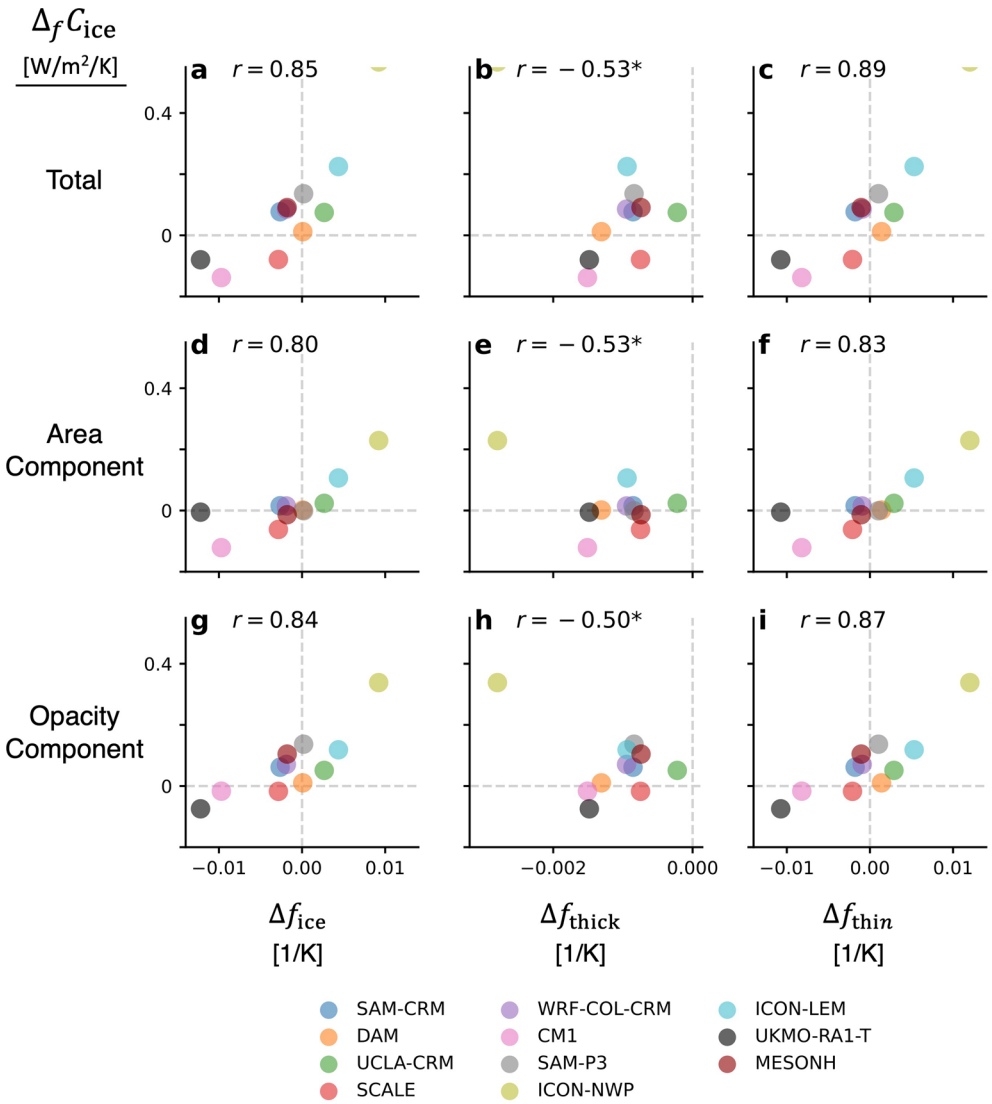

Extended Data Fig. 8 | Relationships between changes in cloud fraction metrics and various radiative feedback components. Changes in f_{ice}, f_{thick}, and f_{thin} versus $\Delta_f C_{ice}$ and its area- and opacity-related components. $\Delta_f C_{ice}$ plotted against **a**, Δf_{ice}; **b**, Δf_{thick}; and **c**, Δf_{thin}. The area component of $\Delta_f C_{ice}$ plotted against **d**, Δf_{ice}; **e**, Δf_{thick}; and **f**, Δf_{thin}. The opacity component of $\Delta_f C_{ice}$ plotted against **g**, Δf_{ice}; **h**, Δf_{thick}; and **i**, Δf_{thin}. Correlation coefficients are shown for each relationship and are marked with an asterisk if *not* statistically different from zero, that is if the 95% confidence interval includes zero (n = 11). All values are normalized by ΔT_s.

https://doi.org/10.1038/s41561-024-01420-6

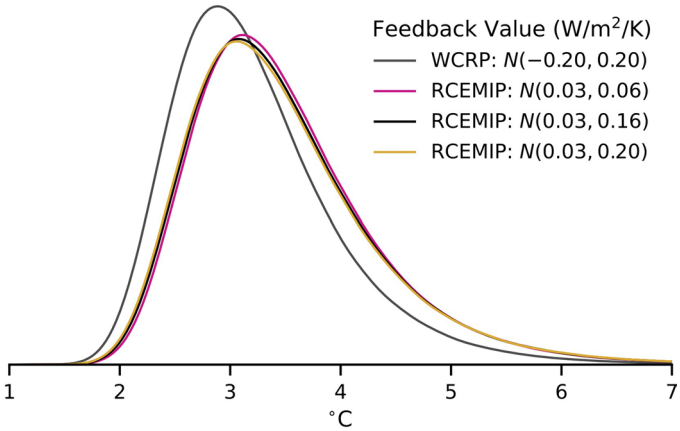

Extended Data Fig. 9 | Sensitivity of the ECS PDF to feedback uncertainty. The test values for the anvil area and opacity feedback are displayed as $N(x, y)$, which represents a Gaussian with mean x and standard deviation y. The three RCEMIP-informed feedback estimates use the same mean value but different standard deviations, which, in increasing order, correspond to the standard deviation of the RCEMIP models, the maximum absolute difference between a single model and multimodel mean, and the original standard deviation assessed by the WCRP.

https://doi.org/10.1038/s41561-024-01420-6

Extended Data Table 1 | Statistics for the posterior PDFs of equilibrium climate sensitivity

Percentile:	5th	17th	50th	83rd	95th	Mode	Mean
WCRP: $N(-0.2, 0.2)$	2.26	2.55	3.11	3.88	4.70	2.96	3.25
RCEMIP: $N(0.03, 0.06)$	2.44	2.77	3.37	4.23	5.11	3.02	3.52
RCEMIP: $N(0.03, 0.16)$	2.41	2.74	3.35	4.22	5.12	3.01	3.50
RCEMIP: $N(0.03, 0.20)$	2.38	2.72	3.33	4.22	5.13	3.11	3.49

Statistics are given for the original WCRP feedback estimate and for the RCEMIP-informed estimates. Each feedback value is reported as a Gaussian of form $N(x, y)$, where x is the mean and y the standard deviation. The three RCEMIP-informed estimates use the same mean value but three different standard deviations, which, in increasing order, correspond to the standard deviation of the RCEMIP ensemble, the maximum deviation of any single model from the multimodel mean, and the original standard deviation assessed by the WCRP.